ARTICLE

www.the-innovation.org

Upgrading heterogeneous Ni catalysts with thiol modification

Pengpeng Ruan,[1,4] Bili Chen,[1,4] Qin Zhou,[2] Hansong Zhang,[1] Yahao Wang,[1] Kunlong Liu,[1] Wenting Zhou,[1] Ruixuan Qin,[1] Zhi Liu,[2] Gang Fu,[1,3,*] and Nanfeng Zheng[1,3,*]

*Correspondence: gfu@xmu.edu.cn (G.F.); nfzheng@xmu.edu.cn (N.Z.)

Received: July 25, 2022; Accepted: December 12, 2022; Published Online: December 14, 2022; https://doi.org/10.1016/j.xinn.2022.100362

GRAPHICAL ABSTRACT

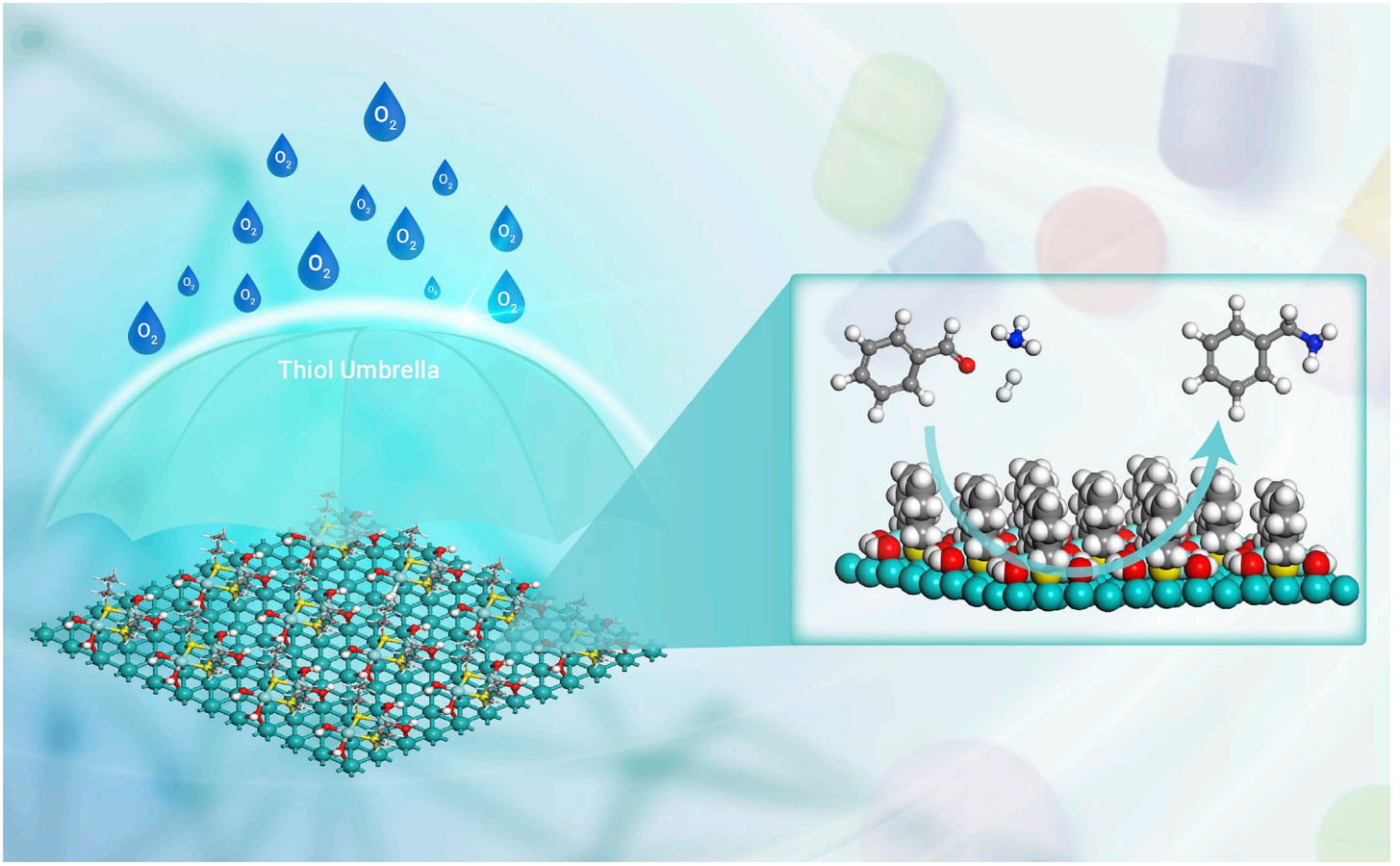

PUBLIC SUMMARY

- Thiol modification of heterogeneous Ni catalysts creates an unexpected promotional effect.
- Improved activity and selectivity in the reductive amination of aldehydes/ketones are achieved.
- Thiol modification prevents the deep oxidation of Ni catalysts and thus improves stability in air.
- A non-contact catalytic mechanism through proton-coupled electron transfer process is revealed.
- The developed thiol modification strategy can be applied to develop low-cost Ni and Co catalysts.

ARTICLE

Upgrading heterogeneous Ni catalysts with thiol modification

Pengpeng Ruan,[1,4] Bili Chen,[1,4] Qin Zhou,[2] Hansong Zhang,[1] Yahao Wang,[1] Kunlong Liu,[1] Wenting Zhou,[1] Ruixuan Qin,[1] Zhi Liu,[2] Gang Fu,[1,3,*] and Nanfeng Zheng[1,3,*]

[1]State Key Laboratory for Physical Chemistry of Solid Surfaces, Collaborative Innovation Center of Chemistry for Energy Materials, and Department of Chemistry, National and Local Joint Engineering Research Center of Preparation Technology of Nanomaterials, College of Chemistry and Chemical Engineering, Xiamen University, Xiamen 361005, China

[2]School of Physical Science and Technology, ShanghaiTech University, Shanghai 201210, China

[3]Innovation Laboratory for Sciences and Technologies of Energy Materials of Fujian Province (IKKEM), Xiamen 361102, China

[4]These authors contributed equally

*Correspondence: gfu@xmu.edu.cn (G.F.); nfzheng@xmu.edu.cn (N.Z.)

Received: July 25, 2022; Accepted: December 12, 2022; Published Online: December 14, 2022; https://doi.org/10.1016/j.xinn.2022.100362

Citation: Ruan P., Chen B., Zhou Q., et al., (2023). Upgrading heterogeneous Ni catalysts with thiol modification. The Innovation **4(1)**, 100362.

Precious metal catalysts are the cornerstone of many industrial processes. Replacing precious metal catalysts with earth-abundant metals is one of key challenges for the green and sustainable development of chemical industry. We report in this work a surprisingly effective strategy toward the development of cost-effective, air-stable, and efficient Ni catalysts by simple surface modification with thiols. The as-prepared catalysts exhibit unprecedentedly high activity and selectivity in the reductive amination of aldehydes/ketones. The thiol modification can not only prevent the deep oxidation of Ni surface to endow the catalyst with long shelf life in air but can also allow the reductive amination to proceed via a non-contact mechanism to selectively produce primary amines. The catalytic performance is far superior to that of precious and non-precious metal catalysts reported in the literature. The wide application scope and high catalytic performance of the developed Ni catalysts make them highly promising for the low-cost, green production of high-value amines in chemical industry.

INTRODUCTION

The development of industrial heterogeneous catalysts using Earth-abundant metals (eg, Ni, iron) has attracted increasing research attention[1–13] but heavily suffers from their easy air oxidation and thus deactivation. With no doubt, the surface modification is expected to provide an effective strategy to enhance their catalytic performance with long shelf life in air by the electronic effect or steric hindrance of organic ligand.[14–21] In the field of heterogeneous catalysis, thiols have been generally considered as poisoning agents for metal catalysts and are only used when necessary to improve the catalytic selectivity. However, by using Ni nanocrystals with well-defined exposure surface as the model catalyst, we demonstrate in this work that the thiol modification not only prevents the oxidative deactivation of the Ni surface to allow the catalyst to be highly stable with long shelf life in air but also induces an unexpected non-contact hydrogenation mechanism to improve the catalytic selectivity toward primary amines. More importantly, the simple thiol modification strategy can be well extended to various Ni nanomaterial systems (ie, Raney Ni, supported Ni nanoparticles, and even Ni carbide) to fabricate cost-effective practical Ni catalysts toward the green synthesis of a wide range of functional primary amines via the reductive amination of aldehydes or ketones.[22–29]

RESULTS AND DISCUSSION

Fabrication and catalytic performance of thiol-modified Ni nanocrystals

In this work, Ni nanocrystals with well-defined exposure surface were first synthesized via thermolysis of Ni acetylacetonate in the presence of oleylamine in 1-octadecene.[30] Transmission electron microscopy (Figure 1A) and X-ray diffraction (Figures S1 and S2) analyses revealed that the as-obtained Ni nanocrystals (denoted as Ni NCs) had a nanoplate morphology with hexagonal close-packed (hcp) crystal structure. The major exposure surface of the NCs is hcp Ni(0001) with Ni atoms in two-dimensional close packing. The Ni NCs were then surface modified with thiols by immersing them in a solution of thiol (eg, 1-octanethiol, 1-butanethiol). It should be noted that the hcp lattice of the Ni NCs after the thiol modification was well maintained (Figures S1E, S1F, and S2). Such a situation is different from the case for the Pd nanosheets treated with aromatic thiol in which the amorphization of Pd lattice caused by S doping was clearly observed.[20] The presence of thiols on the Ni NCs was confirmed by X-ray photoelectron spectroscopy (XPS) and thermogravimetric analysis. While the XPS spectrum of the Ni NCs modified with 1-octanethiol (denoted as Ni–SC_8 NCs) exhibited an obvious doublet S 2p peak that can be assigned to chemisorbed thiolate species (Figure S3),[31] the thermogravimetric analysis revealed an obviously enhanced loss weight at 250°C due to the presence of thiols (Figure S4).

To evaluate whether the thiol modification would modulate the catalytic performance of Ni NCs, the reductive amination of benzaldehyde was chosen as the target reaction owing to its industrial value and complexity with multiple side reactions involved (Figure 1B). Ni NCs were supported on MgO to avoid aggregation during catalysis (Figures S5, S6, and S7). As shown in Figure 1C, while the unmodified Ni NCs gave a yield of 52% to benzylamine, the Ni–SC_8 NCs prepared with modification time of 7 h offered a surprisingly improved yield of 96% under the same condition. Such a catalytic performance was far superior to that of commercial noble metal catalysts (eg, Ru/C, Pd/C) that exhibited a very poor selectivity (<40%) toward benzylamine (Figures 1D and 1E and S8), which can be explained by the enhanced hydrogenation of C=O over the Ru/C or Pd/C catalyst.

Unexpectedly, the catalytic performance of thiol-modified Ni NCs was even positively correlated with the surface thiolate coverage, which was estimated by the combined characterizations of S/Ni ratio by inductively coupled plasma optical emission spectroscopy and the surface Ni dispersion by CO titration (Figure S9). As illustrated in Figure S10A, while the surface thiolate coverage reached the highest level at ~20% at the modification time of 5 h, the as-modified Ni–SC_8 catalyst achieved the highest catalytic activity with the apparent activation energy of *N*-methyl-1-phenylmethanimine hydrogenation greatly reduced from 64 to 27 kJ/mol (Figures 1E and 1F and S11). No poisoning in the activity was revealed even if the modification time was increased up to 7 h using 1 equiv of thiol for the modification (Figure S10B).

While not poisoning Ni NCs, the thiol modification rendered the catalyst with extremely high selectivity toward the production of primary amine in the reductive amination of benzaldehyde. The competitive side reactions, ie, the hydrogenation of benzaldehyde to benzyl alcohol and condensation product dimer to secondary amine, were almost shut down after the thiol modification (Figures S12 and S13). The promoting effect of the thiol modification on both activity and selectivity toward the production of primary amine is unprecedented. It should be noted that the enhanced catalysis reported in this work was not merely observed for specific thiol. Different thiols (eg, 1-butanethiol, benzenethiol) were also successfully used for the surface modification to create catalysts with significantly enhanced performance (Figure S14). With the use of only 3.9 equiv of ammonia, the Ni–SC_8 catalyst displayed a turnover frequency (TOF) of 47.8 h^{-1} at 80°C under 15 atm H_2, much higher than those of non-noble metal catalysts reported in the literature (Table S1).[26–29] Moreover, the Ni–SC_8 catalyst was successfully applied to catalyze the reductive amination of a wide range of aromatic or non-aromatic aldehydes/ketones bearing different functional groups (Figure S15). The Ni–SC_8 catalyst exhibited an excellent stability with no decay in both selectivity and activity after recycling (Figure S16A).

Structure characterizations of thiol-modified Ni catalysts

What was not expected, however, is that if the Ni NCs were pre-reduced by H_2 (80°C, 3 atm H_2, 2 h) before the thiol modification, the as-obtained Ni–H_2–SC_8 catalyst exhibited an extremely poor activity for the reductive amination (Figure 1C). Therefore, the presence of surface Ni(II) species before modification was critical to prevent thiol poisoning. The characteristic absorption peak at 407.4 nm of the UV-visible spectrum proved the existence of Ni(II)–SR complexes in modification solution (Figure S17). As revealed by Raman spectra, the appearance of vibration peaks below 400 cm^{-1} suggested the formation of Ni(II)–SR

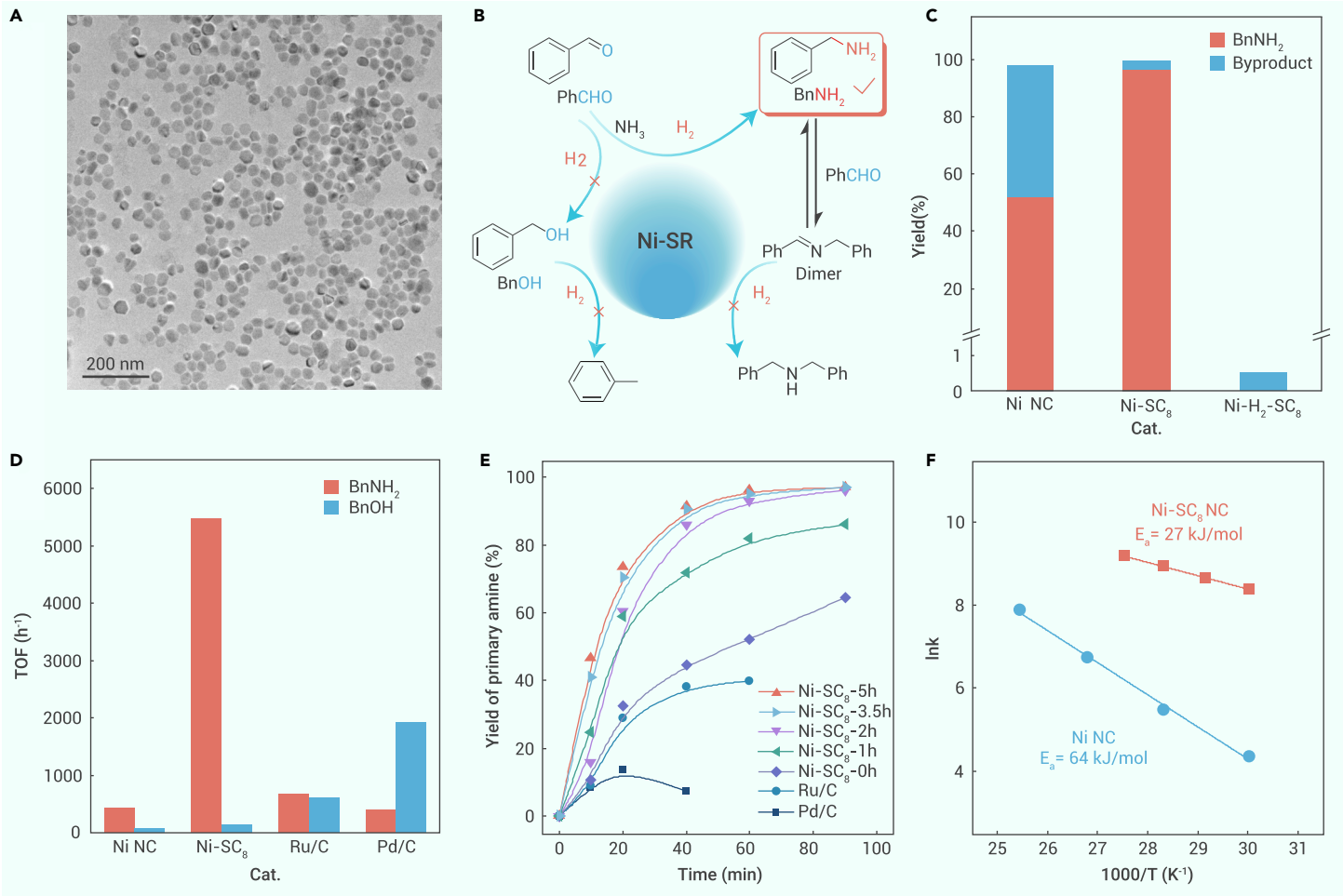

Figure 1. Structure characterizations and hydrogenation performance of thiol-modified Ni nanocrystals (A) TEM image of Ni–SC_8 NCs. (B) The possible reaction pathways for the reductive amination of benzaldehyde catalyzed by Ni–SR NC. (C) The product distribution of benzaldehyde reductive amination catalyzed by Ni NCs, air-oxidized Ni NCs modified by *n*-octanethiol (Ni–SC_8), H_2 pre-reduced Ni NCs modified by *n*-octanethiol (Ni–H_2–SC_8) after reacting for 60 min. (D) The TOF of benzaldehyde reductive amination catalyzed by Ni NCs, air-oxidized Ni NCs modified by *n*-octanethiol (Ni–SC_8) and 5 wt % Ru/C and Pd/C. TOF is calculated based on metal dispersion and at the reaction time of 40 min except the Pd/C is 20 min. (E) Hydrogenation performance for Ni–SC_8 NCs with different modification times, and Ru/C and Pd/C catalysts. Reaction condition: 1 mmol aldehyde, 23 mg catalyst for Ni and 10.6 mg catalyst for Ru/C and Pd/C, 3 mL ethanol, 300 μL 25 wt % ammonium hydroxide, 1 mL H_2O, 80°C, 1.5 MPa H_2. (F) Apparent activation energy of *N*-methyl-1-phenyl-methanimine hydrogenation on the Ni nanocrystal catalysts with and without thiol modification.

bonds upon the surface of Ni–SC_8 NCs (Figure 2A). These results indicated that the surface oxide species was leached partially and that the tetracoordinate planar Ni(II)–SR motifs like Ni(II) thiolate complexes were generated with the thiol modification.

Besides thiolates, the presence of surface O species was revealed on the Ni–SC_8 catalyst by *in situ* XPS measurements under H_2 atmosphere (Figure 2B). While there was no obvious O signal of lattice NiO (normally at 529.4 eV), four different types of oxygen species, ie, physically adsorbed H_2O, surface Ni–O and Ni–OH species, and OH species bound on Ni(II)–SR, were observed on Ni–SC_8 at room temperature. Under 5 mbar H_2, when the temperature was raised to 100°C, the XPS signals of surface Ni–O and Ni–OH disappeared with the increased signal of physically adsorbed H_2O, and at the same time, the content of surface Ni(II) was also reduced (Figures 2C and 2D). Those results suggest the chemical reduction of surface Ni–O and Ni–OH species happened under H_2. However, the OH species bounded on Ni(II)–SR existed in great quantity on the Ni–SC_8 surface (Figure 2D) and surprisingly even survived at 200°C, well consistent with the presence of Ni(II) in the XPS spectra (Figure S18). In sharp contrast, the OH and Ni(II) signals of Ni NCs/nanoparticles without thiol modification disappeared upon H_2 treatment at 200°C, although an intense lattice NiO signal was observed at room temperature (Figures S19, S20, and S21). Those results indicated the thiol can stabilize surface Ni–OH under H_2 at high temperature. Similarly, an obvious optical density vibration signal was detected on Ni–SC_8 NCs under D_2 (1 atm) at 80°C by the *in situ* Fourier transform infrared spectra (Figure S22).

Taking all these together, the presence of NiO species was important to the formation of Ni(II)–SR motifs during the thiol modification process. The as-generated surface Ni(II)–SR motifs helped to not only effectively suppress the deep oxidation of Ni surface in air into NiO but also to stabilize surface OH species on Ni surface under H_2 at elevated temperatures. More importantly, the presence of Ni(II)–SR motifs did not prevent the access and activation of small molecules such as H_2, D_2, and CO (Figure S23). As illustrated in Figure 2E, although the metallic Ni surface on Ni–SC_8 might be slightly oxidized upon air exposure, the presence of Ni(II)–SR motifs helped to prevent the deep oxidation of metallic Ni so that the oxidized Ni surface was readily recovered to a catalytically metallic surface after H_2 treatment under mild conditions.

Mechanistic insights into the promotional effect of thiol modification

To understand how the thiol modification played a critical role in the catalysis, we carried out spin-polarized density functional theory (DFT) calculations using the Venna Ab initio Simulation Package.[32] A (3 × 4) periodic supercell of four-layer hcp Ni(0001) slab with the surface covered by $Ni_2(\mu_2\text{-}RS)_2(OH)_4$ motifs (Figures 2E and S24) at 1/6 thiol coverage was built by considering the following facts: (1) Ni NCs had hcp Ni(0001) as the major exposure surface; (2) the surface thiol coverage was estimated to be ~20%; (3) Ni(II)–SR complexes favor the square planar coordination geometry; and (4) abundant OH species bound on Ni(II)–SR motifs were revealed by XPS. Although hcp Ni(0001) is quite fully covered by $Ni_2(\mu_2\text{-}RS)_2(OH)_4$ motifs at the thiol coverage of 1/6, H_2 can still access the metallic Ni surface underneath (Figure S25). Consistent with the experimental results, the imine and aldehyde were not accessible to metallic Ni surface

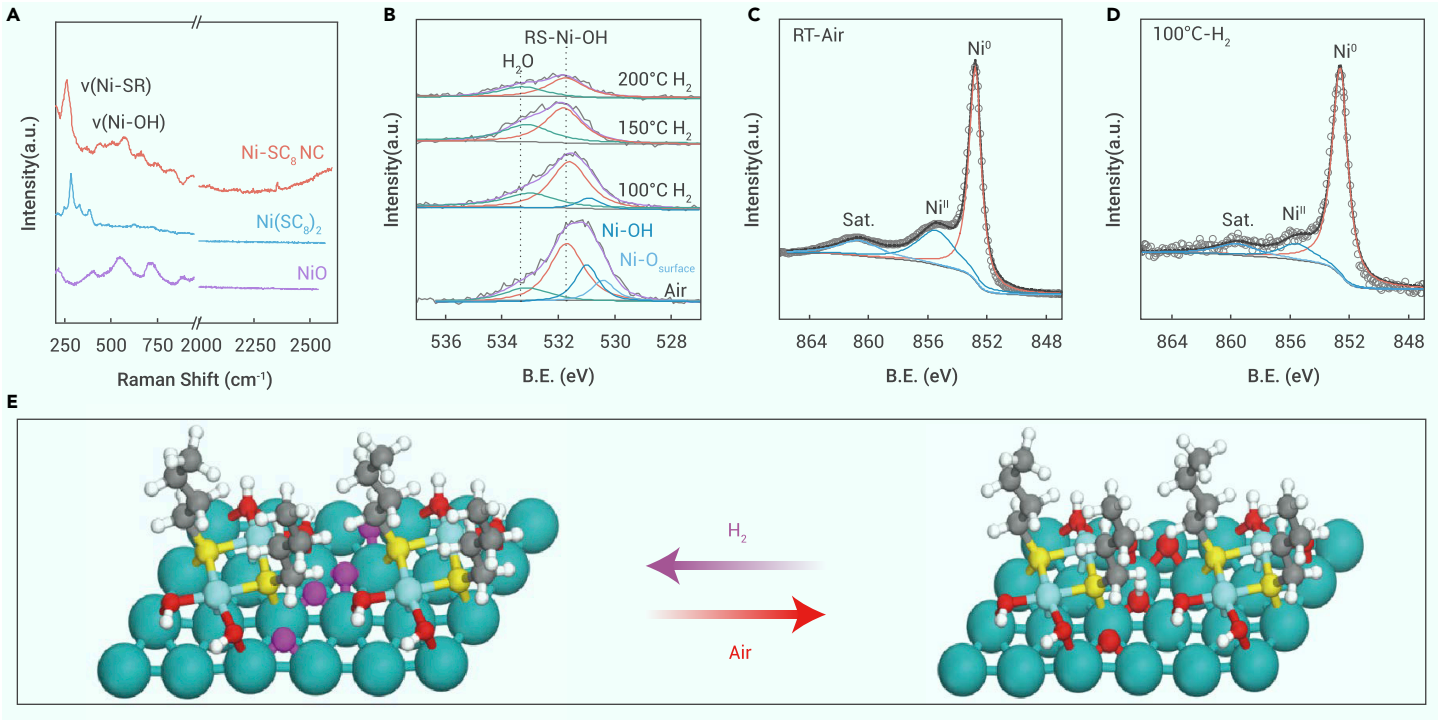

Figure 2. Surface structure of the thiol-modified Ni NC catalyst (A) Raman spectra of Ni-SC_8 NCs, $Ni(SC_8)_2$ complex, and NiO. (B) *In situ* XPS O 1s spectra of Ni–SC_8 NCs treated at different temperatures under H_2 atmosphere. (C) The Ni $2p_{3/2}$ XPS of freshly prepared Ni–SC_8 NCs. (D) *In situ* Ni $2p_{3/2}$ XPS of Ni–SC_8 NCs under H_2 atmosphere at 100°C. (E) Structure illustration of thiol-modified Ni surface upon air oxidation (up) and H_2 treatment (down). Color legend: Ni in cyan and dark cyan, S in yellow, O in red, C in gray, and H in white and pink.

underneath the $Ni_2(\mu_2\text{-}RS)_2(OH)_4$ motifs, so the non-contact hydrogenation mechanism was proposed for the reductive amination on the thiol-modified Ni surface.

In the non-contact mechanism, the hydrogenation occurs between the reactant and the OH groups of $Ni_2(\mu_2\text{-}RS)_2(OH)_4$ motifs, while the metallic Ni still plays the key roles in activating H_2 to deliver activated hydrogen species. Considering the easy reaction of NH_3 with aldehyde to yield imine, the high selectivity toward primary amine in the reductive amination of aldehyde is related to the preferential hydrogenation of the C=N bond in imine on the thiol-modified Ni surface over the C=O bond in aldehyde. Indeed, our calculations suggested that the first-step hydrogenation of benzenemethanimine was thermodynamically more favorable than benzaldehyde over hcp Ni(0001) modified with $Ni_2(\mu_2\text{-}RS)_2(OH)_4$ motifs (Figure 3A). While the hydrogenation on the O end of benzaldehyde was strongly endothermic by 0.98 eV, the hydrogenation on the N end of benzenemethanimine was slightly endothermic by 0.17 eV. Such a large energy difference can be

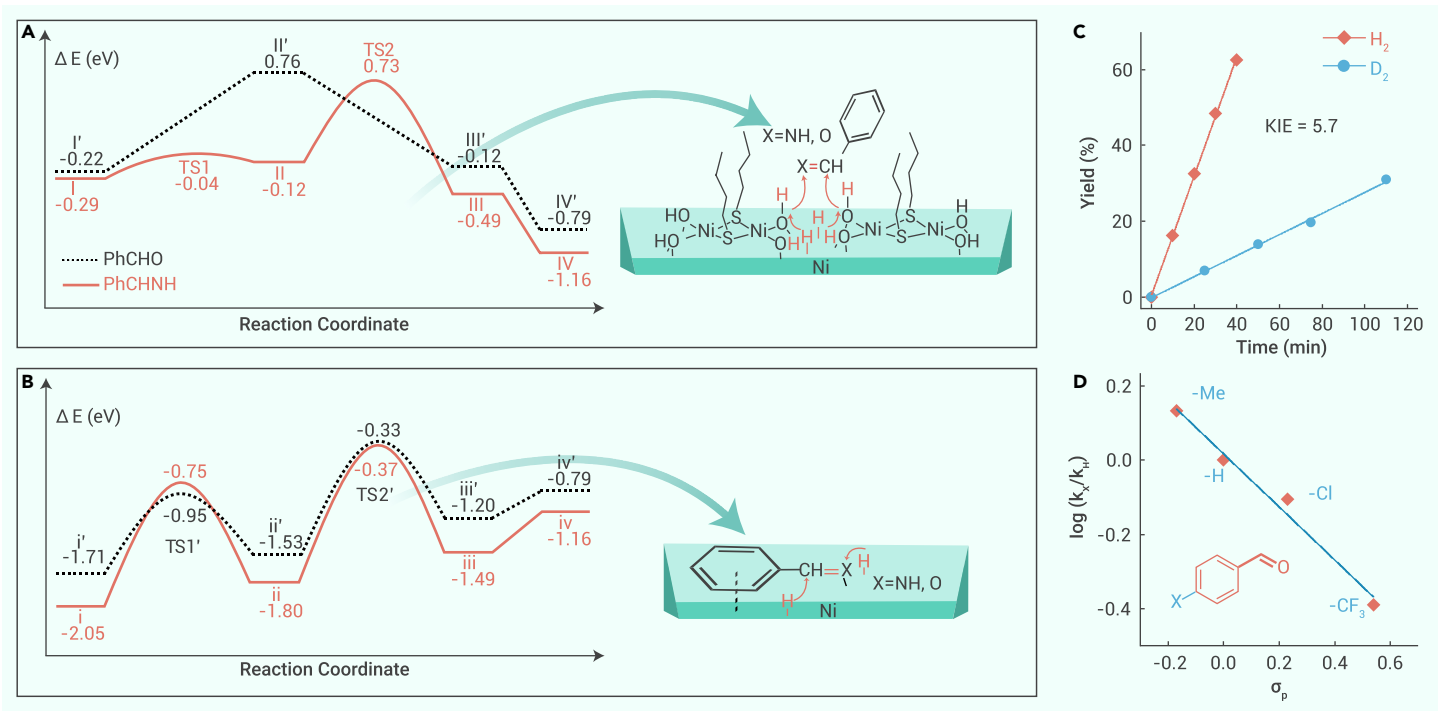

Figure 3. Mechanism for the preferential hydrogenation of imines on the thiol-modified Ni catalyst (A) Non-contact mechanism of benzenemethanimine and benzaldehyde hydrogenation on thiol-modified Ni(0001). (B) Horiuti–Polanyi mechanism of benzenemethanimine and benzaldehyde hydrogenation on Ni(0001) surface. (C) Kinetic isotope effect of Ni–SC_8 catalyzed hydrogenation of *N*-benzylidene methylamine. (D) Hammett plot of Ni–SC_8 catalyzed reductive amination of benzaldehydes with different functional groups.

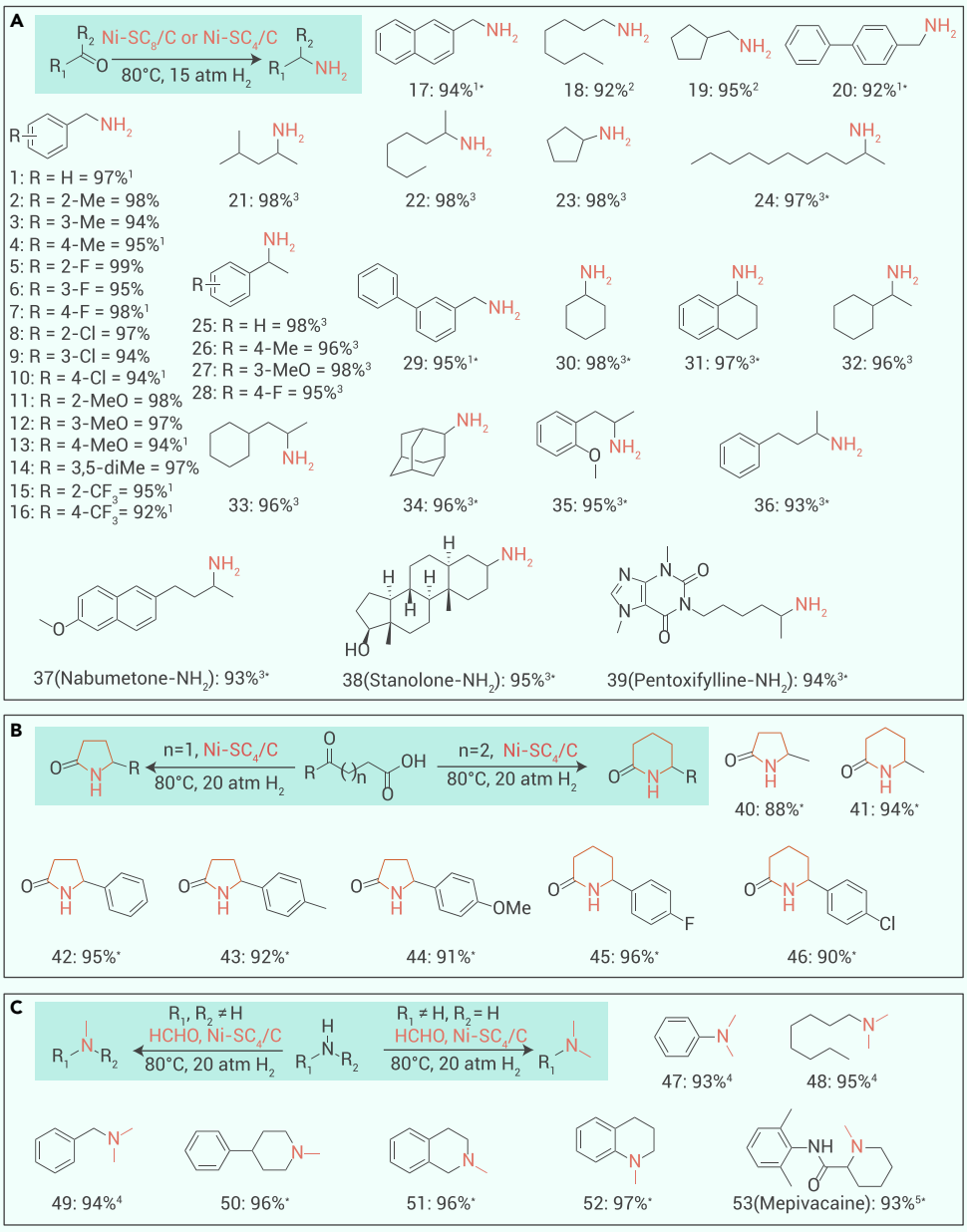

Figure 4. Wide substrate scope for the reductive amination catalyzed by thiol-modified Ni/C catalyst

(A) Reductive amination of aldehydes and ketones. Conditions: 2 mmol substrate, 6 mg 20 wt % Ni–SC_8/C (1 mol % Ni, thiol modification time 5 h), 1 mL NH_3·H_2O (25 wt %, 13 mmol), 3 mL MeOH, 80°C, 15 atm H_2, and 3 h. The GC yield was based on carbonyl compound. Condition 1: 12 mg 20 wt % Ni-SC_8/C (2 mol % Ni, thiol modification time 5 h), 1.5 mL NH_3·H_2O (20 mmol). Condition 2: 30 mg 20 wt % Ni-SC_4/C (5 mol % Ni, thiol modification time 5 h), reaction time is 30 min. Condition 3: 18 mg 20 wt % Ni–SC_4/C (3 mol % Ni, thiol modification time 5 h), 2 mL 7 M NH_3 methanol solution (14 mmol NH_3) and 2 mL methanol, 80°C, 20 atm H_2, and 3 h. (B) Reductive amination of keto acid. Conditions: 2 mmol substrate, 21 mg 20 wt % Ni–SC_4 /C (3.5 mol % Ni, thiol modification time 3 h), 2 mL 7 M NH_3 methanol solution (14 mmol NH_3), and 4 mL methanol, 80°C, 20 atm H_2, and 3 h. (C) Reactions of amines with formaldehyde in H_2. Conditions: 2 mmol substrate, 6 mg 20 wt % Ni–SC_4/C (1 mol % Ni, thiol modification time 1 h), 400 to 800 μl formaldehyde aqueous formaldehyde (37%) (4.0 equiv for primary amine and 2.0 equiv for secondary amine), 80°C, 20 atm H_2, 2 h. The GC yield was based on amine using dodecane as internal standard. Condition 4: 2 mol % Ni, reaction time is 3 h. Condition 5: 3.5 mol % Ni, reaction time is 24 h. An asterisk (*) indicates isolated yield.

explained by the fact that the C=N bond is weaker than the C=O bond. In addition, the first H addition on benzenemethanimine can be stabilized by forming a favorable $O^{\delta-}\cdots H^{\delta+}\cdots N^{\delta-}$ structure (Figures S26 and S27).

DFT calculations showed that the first and second H additions for benzenemethanimine need to surmount only 0.25 and 0.85 eV barriers on the thiol-modified surface. The consumed (NiO)–H species can be replenished by H atoms on the metallic Ni surface by overcoming an energy barrier of ~0.8 eV (Figure 3A, S28 and S29). These findings nicely explain why the Ni–SC_8 catalyst exhibited high hydrogenation activity. Moreover, the steric hindrance caused by the thiol modification would prevent the hydrogenation of dimer from being hydrogenated to secondary amine (Figure 2B). In contrast to the non-contact mechanism on thiol-modified Ni(0001), the hydrogenation on Ni(0001) still followed the Horiuti–Polanyi mechanism, in which two H atoms would add into the unsaturated C=X bonds one by one. (Figures 3B, S30 and S31). Bader charge analysis showed that the H atoms on Ni(0001) were negatively charged by −0.25 a.u., different from positively charged (NiO)–H species on the thiol-modified Ni(0001). Thus, the hydrogenation on Ni(0001) and thiol-modified Ni(0001) should exhibit different chemoselectivity. As shown in Figure 3A, the hydrogenation of benzenemethanimine and benzaldehyde on Ni(0001) would be competitive and need to overcome relatively high barriers in TS2′ (1.2–1.4 eV), explaining the experimental observation of poor selectivity and poor activity on Ni NCs. Thus, both electronic and steric effects render the thiol-modified Ni catalyst with high activity and high selectivity toward primary amine.

The proposed non-contact mechanism was verified by the large kinetic isotope effect of 5.7 for the *N*-methyl-1-phenylmethanimine hydrogenation catalyzed by the thiol-modified Ni catalyst (Figure 3C and S32). Moreover, the Hammett plot against σ(p) displayed a linear relationship with a negative slope,[33] confirming that the imine hydrogenation involved slightly more proton-transfer than electron-transfer character as expected from the proton-coupled electron transport mechanism (Figures 3D and S33).[34,35] As expected, the hydrogenation of benzonitrile on the thiol-modified Ni catalyst was suppressed, although the unmodified Ni catalyst exhibited reasonable activity (Figure S34). While a slower reaction rate was observed over the Ni catalyst, the reductive amination of 2-methylbenzaldehyde with larger steric hindrance proceeded faster than benzaldehyde over the Ni–SC_8 catalyst (Figure S35). All these results confirmed that the non-contact mechanism can account for the unique selectivity in imine hydrogenation catalyzed by the thiol-modified Ni catalyst.

DFT calculations also suggested that the deep oxidation of Ni can be effectively suppressed by the presence of surface Ni–SR motifs (Figures S36 and S37). Such a capability is important to fabricate air-stable Ni catalysts for practical applications. As demonstrated by both DFT calculations (Figure S38) and *in situ* XPS measurements discussed above (Figures 2C and 2D), H_2 can still be activated to reduce surface oxide species and further regenerate the metallic Ni surface, although the Ni surface might be slightly oxidized in air. Considering that Ni nanocatalysts, for example Raney Ni, are highly flammable and easily deactivated in air due to the formation of a continuous oxide passivating layer, such surface reactivity of the thiol-modified Ni surface is crucial to endow Ni catalysts with a long shelf life without special storage conditions in air. Indeed, the Ni(II) XPS signal of the Ni–SR catalyst stored in air for 30 days displayed a similar intensity to that for 15 days (Figure S39). No obvious decay in the catalytic performance was revealed on the Ni–SR catalyst stored in air for different periods (Figure S40).

Application of the modification strategy to create low-cost catalysts

Most importantly, the strategy developed in this work is applicable to modify Ni catalysts in different forms, eg, low-cost supported Ni/C catalyst (Figure S41) and Ni carbide (Figures S42, S43, and S44) and even supported Co/C catalyst. The thiol-modified Ni and cobalt catalysts displayed higher activity and amine selectivity (95.3%–97.1%) than their unmodified counterparts (75.6%–82.9%) (Figures S45 and S46). As demonstrated in Figure 4, with the use of the thiol-modified Ni/C catalyst, a wide range of primary amines have been successfully synthesized in high yield and selectivity via the reductive amination of their ketone or aldehyde counterparts under mild conditions, providing a green alternative to the industrial production of amines.

METHODS

Preparation of hcp Ni NC

240 mg $Ni(acac)_2$ was added into a mixture containing 1.6 mL oleylamine and 8 mL 1-octadecene in Ar atmosphere. After stirring for 30 min, the solution was heated up to 240 °C and then kept at the temperature for 20 min under Ar flow (80 mL/min). The black solution was naturally cooled to room temperature and washed with ethanol and n-hexane several times. The as-obtained hcp Ni NCs was further dispersed in ethanol for the thiol modification. To be used in catalysis, the hcp Ni NCs were supported on MgO, ZnO or TiO_2 to prevent their aggregation.

Preparation of carbon-supported 20 wt% Ni catalyst

The 20 wt% Ni/C supported catalyst was synthesized through the hydrogen thermal reduction method. In a typical synthesis, $Ni(NO_3)_2 \cdot 6H_2O$ (1.0 g) was dissolved in 30 mL ethanol. 0.8 g of carbon support was then added into the solution. The mixed solution was evaporated to dryness at 75 °C. The residual black solid was then heated to 400 °C at a rate of 4 $K \cdot min^{-1}$ and kept at 400 °C for 120 min under 5% H_2/Ar flow (80 mL/min). After cooled naturally to room temperature, the as-obtained Ni/C catalyst was purged with nitrogen (80 mL/min) for 60 min and then air (20 mL/min) for 3 min. The as-synthesized Ni/C catalyst was modified with thiol immediately.

Thiol-modified Ni catalyst

The pre-made Ni nanomaterials were dispersed in the ethanol solution of thiol with the molar ratio of Ni/thiol of 1. The concentration of thiol solution used for the modification was 0.1 M. The mixture was stirred over a certain period at 45 °C under N_2 to make sure that thiol was adsorbed on the surface of Ni. After the modification, the thiol-modified Ni-SR NCs were separated by centrifugation and washed several times by ethanol and n-hexane. The as-obtained Ni-SR NCs were further loaded on metal oxide supports (MgO, ZnO or TiO_2) with 5 wt% loading to prevent the aggregation of Ni NCs.

Reductive amination of aldehyde

In a typical reaction, aldehyde (3 mmol), ammonia (1 mL, 13 mmol) and Ni catalyst (2 mol% Ni, modification time 5 h) were fully mixed in 9 mL methanol by ultrasonication. The mixture was then placed in a 25 mL Teflon lined high-pressure reactor which was flushed three times by H_2. The H_2 pressure was adjusted to 1.5 MPa for the catalysis. After the reaction was stirred at 80 °C for certain time, 100 μL reaction solution was taken out with pipette to monitor the reaction progress using GC-MS. After the reaction, the mixture was centrifuged to collect the solution phase. The crude mixture was purified by flash column chromatography on silica gel to give the primary amine product.

Reductive amination of ketone

In a typical reaction, ketone (2 mmol), 2 mL of 7 M ammonia in methanol (14 mmol), and Ni catalyst (3 mol% Ni, modification time 3 h) were fully mixed in 2 mL methanol by ultrasonication. The mixture was then placed in a 25 mL Teflon lined high-pressure reactor which was flushed three times by H_2. The H_2 pressure was adjusted to 2.0 MPa for the catalysis. After the reaction was stirred at 80 °C for certain time, 100 μL reaction solution was taken out with pipette to monitor the reaction progress through GC-MS. After the reaction, the mixture was centrifuged to collect the solution phase. The crude mixture was purified by flash column chromatography on silica gel to give the alcohol product.

Reductive amination of keto acid

In a typical reaction, keto acid (2 mmol), 2 mL of 7 M ammonia in methanol (14 mmol), and Ni catalyst (3.5 mol% Ni, modification time 3 h) were fully mixed in 3 mL methanol by ultrasonication. The mixture was then placed in a 25 mL Teflon lined high-pressure reactor which was flushed three times by H_2. The H_2 pressure was then adjusted to 2.0 MPa for the catalysis. After the reaction was stirred at 80 °C for certain time, 100 μL reaction solution was taken out with pipette to monitor the reaction progress through GC-MS. After the reaction, the mixture was centrifuged to collect the solution phase. The crude mixture was purified by flash column chromatography on silica gel to give the amine product.

Reaction of amine with formaldehyde

In a typical reaction, amine (2 mmol), 280 to 560 uL of aqueous formaldehyde (37%) (5.6 mmol for primary amine, 2.8 mmol for secondary amine), and Ni catalyst (1 mol% Ni, modification time 1 h) were fully mixed in 3 mL methanol by ultrasonication. The mixture was then placed in a 25 mL Teflon lined high-pressure reactor which was flushed three times by H_2. The H_2 pressure was adjusted to 2.0 MPa for the catalysis. After the reaction was stirred at 80 °C for certain time, 100 μL reaction solution was taken out with pipette to monitor the reaction progress through GC-MS. After the reaction, the mixture was centrifuged to collect the solution phase. The crude mixture was purified by flash column chromatography on silica gel to give the amine product.

Hydrogenation of aldehyde

In a typical reaction, aldehyde (1 mmol), 12 mg of 5wt% Ni NC/MgO or Ni-SC_8 NC/MgO (1 mol% Ni) were added in 5 mL ethanol, which was then placed in a 25 mL Teflon Lined high-pressure reactor and flushed three times by H_2. The H_2 pressure was adjusted to 1.5 MPa for the catalysis. After the reaction was stirred at 80 °C at certain time, 100 μL reaction solution was taken out with pipette to monitor the reaction progress through GC-MS.

Hydrogenation of imine

In a typical reaction, imine (1 mmol), 12 mg of 5wt% Ni NC/MgO or Ni-SC8 NC/MgO (1 mol% Ni) were added into 5 mL ethanol solution, which was then placed in a 25 mL Teflon Lined high-pressure reactor and flushed three times by H_2. The H_2 pressure was then adjusted to 1.5 MPa for the catalysis. After the reaction was stirred at 80 °C at certain time, 100 μL reaction solution was taken out pipette to monitor the reaction progress through GC-MS.

Hydrogenation of nitrile

In a typical reaction, nitrile (1 mmol), 12 mg of 5wt% Ni NC/MgO or Ni-SC_8 NC/MgO (1 mol% Ni) mixed with 5 mL ethanol were added into a 25 mL Teflon Lined high-pressure reactor. The H_2 pressure was adjusted to 1.5 MPa for the catalysis. After the reaction was stirred at 80 °C at certain time, 100 μL reaction solution was taken out with pipette to monitor the reaction progress through GC-MS.

CONCLUSION

In conclusion, we have developed an effective thiol-modification strategy to adjust the aldehyde/ketone reductive amination performance of Ni-based catalysts. Detailed studies demonstrated the thiol modification of Ni NCs with partially oxidized surfaces led to the formation of unique HO–Ni(II)–SR surface motifs, which can survive at elevated temperatures under H_2 and further assist the proton transfer from the metallic Ni surface to imines without the need of contacting metallic Ni sites. Such an unexpected non-contact hydrogenation mechanism greatly reduced the apparent activation energy of imine hydrogenation but shut down the hydrogenation of the C=O bond or dimer due to the huge steric hindrance of thiol. Therefore, both activity and selectivity toward primary amines were obviously improved via the simple thiol modification. Moreover, the as-generated surface Ni(II)–SR motifs can effectively suppress the deep oxidation of Ni so that the Ni–SR catalyst can be stored in air for 30 days with no obvious decay of catalytic activity. Most importantly, the simple modification strategy can be easily extended to other heterogeneous catalysts based on Ni and Co. With the possible production of low-cost carbon-supported Ni/C or Co/C catalysts in large scale, the cost-effective preparation of bioactive amine drugs via the reductive amination of aldehydes/ketones with the use of air-stable non-precious metal catalysts is expected to be achieved in the future.

REFERENCES

1. Bullock, R.M., Chen, J.G., Gagliardi, L., et al. (2020). Using nature's blueprint to expand catalysis with Earth-abundant metals. Science ***369***, eabc3183.
2. Filonenko, G.A., van Putten, R., Hensen, E.J.M., and Pidko, E.A. (2018). Catalytic (de)hydrogenation promoted by non-precious metals - Co, Fe and Mn: recent advances in an emerging field. Chem. Soc. Rev. ***47***, 1459–1483.
3. Jagadeesh, R.V., Surkus, A.E., Junge, H., et al. (2013). Nanoscale Fe_2O_3-based catalysts for selective hydrogenation of nitroarenes to anilines. Science ***342***, 1073–1076.
4. Korstanje, T.J., van der Vlugt, J.I., Elsevier, C.J., and de Bruin, B. (2015). Hydrogenation of carboxylic acids with a homogeneous cobalt catalyst. Science ***350***, 298–302.

5. Song, Y., Ozdemir, E., Ramesh, S., et al. (2020). Dry reforming of methane by stable Ni-Mo nanocatalysts on single-crystalline MgO. Science ***367***, 777–781.
6. Studt, F., Abild-Pedersen, F., Bligaard, T., et al. (2008). Identification of non-precious metal alloy catalysts for selective hydrogenation of acetylene. Science ***320***, 1320–1322.
7. Tasker, S.Z., Standley, E.A., and Jamison, T.F. (2014). Recent advances in homogeneous nickel catalysis. Nature ***509***, 299–309.
8. Wang, D., and Astruc, D. (2017). The recent development of efficient Earth-abundant transition-metal nanocatalysts. Chem. Soc. Rev. ***46***, 816–854.
9. Westerhaus, F.A., Jagadeesh, R.V., Wienhöfer, G., et al. (2013). Heterogenized cobalt oxide catalysts for nitroarene reduction by pyrolysis of molecularly defined complexes. Nat. Chem. ***5***, 537–543.
10. Ye, T.N., Park, S.W., Lu, Y., et al. (2020). Vacancy-enabled N_2 activation for ammonia synthesis on an Ni-loaded catalyst. Nature ***583***, 391–395.
11. Nishimura, S. (2001). Handbook of Heterogeneous Catalytic Hydrogenation for Organic Synthesis (New York: Wiley).
12. Herkes, F.E. (1998). Catalysis of Organic Reactions (CRC Press).
13. Fouilloux, P. (1983). The nature of raney nickel, its adsorbed hydrogen and its catalytic activity for hydrogenation reactions. Appl. Catal. ***8***, 1–42.
14. Zhang, J., Ellis, L.D., Wang, B., et al. (2018). Control of interfacial acid–metal catalysis with organic monolayers. Nat. Catal. ***1***, 148–155.
15. Jenkins, A.H., and Medlin, J.W. (2021). Controlling heterogeneous catalysis with organic monolayers on metal oxides. Acc. Chem. Res. ***54***, 4080–4090.
16. Marshall, S.T., O'Brien, M., Oetter, B., et al. (2010). Controlled selectivity for palladium catalysts using self-assembled monolayers. Nat. Mater. ***9***, 853–858.
17. Chen, G., Xu, C., Huang, X., et al. (2016). Interfacial electronic effects control the reaction selectivity of platinum catalysts. Nat. Mater. ***15***, 564–569.
18. Liu, P., Qin, R., Fu, G., and Zheng, N. (2017). Surface coordination chemistry of metal nanomaterials. J. Am. Chem. Soc. ***139***, 2122–2131.
19. Peng, J., Chen, B., Wang, Z., et al. (2020). Surface coordination layer passivates oxidation of copper. Nature ***586***, 390–394.
20. Zhao, X., Zhou, L., Zhang, W., et al. (2018). Thiol treatment creates selective palladium catalysts for semihydrogenation of internal alkynes. Chem ***4***, 1080–1091.
21. Zhukhovitskiy, A.V., MacLeod, M.J., and Johnson, J.A. (2015). Carbene ligands in surface chemistry: from stabilization of discrete elemental allotropes to modification of nanoscale and bulk substrates. Chem. Rev. ***115***, 11503–11532.
22. Afanasyev, O.I., Kuchuk, E., Usanov, D.L., and Chusov, D. (2019). Reductive amination in the synthesis of pharmaceuticals. Chem. Rev. ***119***, 11857–11911.
23. Murugesan, K., Senthamarai, T., Chandrashekhar, V.G., et al. (2020). Catalytic reductive aminations using molecular hydrogen for synthesis of different kinds of amines. Chem. Soc. Rev. ***49***, 6273–6328.
24. Irrgang, T., and Kempe, R. (2020). Transition-metal-catalyzed reductive amination employing hydrogen. Chem. Rev. ***120***, 9583–9674.
25. Kumar, R., Karmilowicz, M.J., Burke, D., et al. (2021). Biocatalytic reductive amination from discovery to commercial manufacturing applied to abrocitinib JAK1 inhibitor. Nat. Catal. ***4***, 775–782.
26. Jagadeesh, R.V., Murugesan, K., Alshammari, A.S., et al. (2017). MOF-derived cobalt nanoparticles catalyze a general synthesis of amines. Science ***358***, 326–332.
27. Hahn, G., Kunnas, P., de Jonge, N., and Kempe, R. (2019). General synthesis of primary amines via reductive amination employing a reusable nickel catalyst. Nat. Catal. ***2***, 71–77.
28. Murugesan, K., Chandrashekhar, V.G., Senthamarai, T., et al. (2020). Reductive amination using cobalt-based nanoparticles for synthesis of amines. Nat. Protoc. ***15***, 1313–1337.
29. Murugesan, K., Beller, M., and Jagadeesh, R.V. (2019). Reusable nickel nanoparticles-catalyzed reductive amination for selective synthesis of primary amines. Angew. Chem. Int. Ed. Engl. ***58***, 5064–5068.
30. Han, M., Liu, Q., He, J., et al. (2007). Controllable synthesis and magnetic properties of cubic and hexagonal phase nickel nanocrystals. Adv. Mater. ***19***, 1096–1100.
31. Mekhalif, Z., Laffineur, F., Couturier, N., and Delhalle, J. (2003). Elaboration of self-assembled monolayers of n-alkanethiols on nickel polycrystalline substrates: time, concentration, and solvent effects. Langmuir ***19***, 637–645.
32. Hafner, J. (2008). Ab-initio simulations of materials using VASP: density-functional theory and beyond. J. Comput. Chem. ***29***, 2044–2078.
33. Hansch, C., Leo, A., and Taft, R.W. (2002). A survey of Hammett substituent constants and resonance and field parameters. Chem. Rev. ***91***, 165–195.
34. Chalkley, M.J., Garrido-Barros, P., and Peters, J.C. (2020). A molecular mediator for reductive concerted proton-electron transfers via electrocatalysis. Science ***369***, 850–854.
35. Weinberg, D.R., Gagliardi, C.J., Hull, J.F., et al. (2012). Proton-coupled electron transfer. Chem. Rev. ***112***, 4016–4093.

ACKNOWLEDGMENTS

The project was supported by the National Natural Science Foundation of China (21890752, 21731005, 21721001, 22072116, 92045303, 22132004, and 22002126), the National Key R&D Program of China (2017YFA0207302 and 2017YFA0207303), and the fundamental research funds for Central Universities (20720180026). N.Z. acknowledges support from the Tencent Foundation through the XPLORER PRIZE.

AUTHOR CONTRIBUTIONS

N.Z. conceived and supervised the research project. P.R. synthesized and characterized the samples and investigated the catalytic performances. G.F. supervised the DFT calculations and analyzed the computational results together with B.C. Q.Z. and Z.L. contributed to the XPS measurements. H.Z. and Y.W. contributed to the catalyst preparations. K.L. contributed to the Fourier transform infrared measurements. W.Z. and R.Q. contributed the analysis of Hammett plot. N.Z., G.F., P.R., and B.C. wrote and revised the manuscript.

DECLARATION OF INTERESTS

The authors declare no competing interests.

SUPPLEMENTAL INFORMATION

It can be found online at https://doi.org/10.1016/j.xinn.2022.100362.

LEAD CONTACT WEBSITE

http://nfzheng.xmu.edu.cn